PNAS RESEARCH ARTICLE | BIOPHYSICS AND COMPUTATIONAL BIOLOGY

Driving forces of the complex formation between highly charged disordered proteins

Aritra Chowdhury[a,1], Alessandro Borgia[a,2], Souradeep Ghosh[b], Andrea Sottini[a], Soumik Mitra[b], Rohan S. Eapen[a], Madeleine B. Borgia[a,2], Tianjin Yang[a], Nicola Galvanetto[a,c], Miloš T. Ivanović[a], Paweł Łukijańczuk[a], Ruijing Zhu[a], Daniel Nettels[a], Arindam Kundagrami[b,1], and Benjamin Schuler[a,c,1]

Edited by Matthew Tirrell, The University of Chicago, Chicago, IL; received March 14, 2023; accepted August 22, 2023

Highly disordered complexes between oppositely charged intrinsically disordered proteins present a new paradigm of biomolecular interactions. Here, we investigate the driving forces of such interactions for the example of the highly positively charged linker histone H1 and its highly negatively charged chaperone, prothymosin α (ProTα). Temperature-dependent single-molecule Förster resonance energy transfer (FRET) experiments and isothermal titration calorimetry reveal ProTα-H1 binding to be enthalpically unfavorable, and salt-dependent affinity measurements suggest counterion release entropy to be an important thermodynamic driving force. Using single-molecule FRET, we also identify ternary complexes between ProTα and H1 in addition to the heterodimer at equilibrium and show how they contribute to the thermodynamics observed in ensemble experiments. Finally, we explain the observed thermodynamics quantitatively with a mean-field polyelectrolyte theory that treats counterion release explicitly. ProTα-H1 complex formation resembles the interactions between synthetic polyelectrolytes, and the underlying principles are likely to be of broad relevance for interactions between charged biomolecules in general.

intrinsically disordered proteins | single-molecule spectroscopy | protein binding | polyelectrolyte complexation

Significance

Charged disordered proteins are abundant in the cell, especially in the nucleus, and oppositely charged molecules can form high-affinity disordered complexes. Such interactions can exhibit surprising behavior, such as increased affinity with increasing temperature, but a detailed characterization of the underlying thermodynamic driving forces has been lacking. Combining single-molecule FRET (Förster resonance energy transfer), calorimetry, and analytical polymer theory, we dissect the thermodynamics of the disordered high-affinity complex between two highly charged disordered proteins and find that the release of counterions is an essential entropic contribution to binding. Our results also demonstrate the formation of higher-order complexes at high protein concentrations, and provide a quantitative experimental and theoretical framework for elucidating the interactions of charged disordered biomolecules and synthetic polyelectrolytes.

Intrinsically disordered proteins (IDPs) can bind to many different cellular targets and are thus abundant in molecular interaction hubs (1–3). The underlying interaction mechanisms and the extent of disorder in IDP complexes cover a remarkably broad spectrum. For some IDPs, binding is coupled to folding and results in complexes with a well-defined three-dimensional structure (4). In other cases, some disorder is retained in the bound state (5, 6). For instance, IDPs often employ short secondary structure elements, small linear motifs, or even single-site modifications or side chains to engage interaction partners (7, 8). As a result, large parts of the chain can remain disordered. In extreme cases, one or both partners fully retain their structural disorder after binding, a mechanism that is particularly common for highly charged IDPs interacting with each other or with nucleic acids (9–13). We have recently identified such an example, the complex between the two human IDPs prothymosin α (ProTα) and linker histone H1 (13). ProTα and H1 carry large opposite net charges (−44 and +53, respectively) and associate into a heterodimer with picomolar to nanomolar affinity in the physiological range of salt concentrations, yet they retain their disorder in the complex. ProTα acts as a chaperone of H1 (14) and enables the dissociation of H1 from nucleosomes despite the extreme affinity of the H1-nucleosome complex (15).

The surprising absence of structure formation and of structured interaction interfaces in such disordered complexes raises the question of how the underlying thermodynamic driving forces for binding differ from the classical paradigms of interactions for folded proteins (16–18). In many respects, the interactions between highly charged naturally occurring biopolymers are reminiscent of the complexation between synthetic polyelectrolytes (9, 19–22). However, for synthetic systems, it has been challenging to experimentally probe the properties of small oligomers with well-defined stoichiometry separately from their phase separation by complex coacervation (23). The preparative biochemical methods and single-molecule spectroscopy available for biological polyelectrolytes provide an opportunity for closing this gap. Here, we dissect the thermodynamic driving forces involved in the formation of the dimer and the ternary complexes of ProTα and H1 under conditions where phase separation does not occur. We show that in spite of the high affinity, the interaction is enthalpically unfavorable and instead driven by the entropy gain from counterion release, as suggested for polyelectrolyte complexation (9, 19, 21, 22, 24–27).* Considering the abundance of

The authors declare no competing interest.

This article is a PNAS Direct Submission.

[1]To whom correspondence may be addressed. Email: a.chowdhury@bioc.uzh.ch, arindam@iiserkol.ac.in, or schuler@bioc.uzh.ch.

[2]Present address: Department of Structural Biology, St. Jude Children's Research Hospital, Memphis, TN 38105.

This article contains supporting information online at https://www.pnas.org/lookup/suppl/doi:10.1073/pnas.2304036120/-/DCSupplemental.

Published October 5, 2023.

charges in IDPs and other biomolecules in the cell, the thermodynamic characteristics of the ProTα-H1 interaction are likely to resemble those of many biomolecular binding processes.

Results

High Affinity Despite Unfavorable Enthalpy. The most striking feature of the ProTα-H1 complex is that the two IDPs bind to each other with picomolar to nanomolar affinity in the physiological ionic strength range, although they both remain disordered in the complex (13, 28). To enable measurements at the very low protein concentrations where the equilibrium between monomers and the dimer of ProTα (P) and H1 (H) can be monitored, we use single-molecule Förster resonance energy transfer (FRET) on freely diffusing molecules with confocal detection (29–33). ProTα labeled with donor and acceptor fluorophores (Alexa Fluor 488 and 594, respectively) at positions 56 and 110 exhibits a FRET efficiency of 0.37 ± 0.03 at a monovalent salt concentration† of 208 mM. Upon titrating picomolar concentrations of labeled ProTα with increasing concentrations of unlabeled H1, we observe a second population corresponding to the ProTα-H1 dimer (PH) (Fig. 1*A*). Owing to the mutual charge screening of the two oppositely charged IDPs, ProTα is more compact in the complex (13), resulting in a higher transfer efficiency of 0.56 ± 0.03. The equilibrium fraction of PH as a function of H1 concentration allows us to determine the equilibrium dissociation constant, K_D^{PH} (Fig. 1*B*). K_D^{PH} increases from $2.1^{+1.1}_{-0.8}$ pM at 165 mM (13) to $1.2^{+1.2}_{-0.6}$ nM at 208 mM monovalent salt concentration.

To assess the role of enthalpic and entropic contributions to the binding process, we investigated the temperature dependence of K_D^{PH}. We measured transfer efficiency histograms of picomolar concentrations of labeled ProTα in the presence of a fixed concentration of unlabeled H1 close to K_D^{PH} between 283.5 K and 331 K (Fig. 1*C*). The temperature dependence reveals another remarkable feature of the PH complex: The equilibrium fraction of PH increases with increasing temperature, i.e., higher temperature favors binding (Fig. 1*D*). Correspondingly, ProTα-H1 complex formation must be associated with a thermodynamically unfavorable, positive enthalpy change, $\Delta H^{PH} > 0$. This conclusion is confirmed by isothermal titration calorimetry (ITC), which shows the signature of an endothermic reaction (Fig. 1*E*), as observed previously (34). Since $\Delta H^{PH} > 0$, ProTα-H1 binding must be entropically driven. This behavior contrasts with many high-affinity protein interactions, for which the enthalpy of binding is often favorable (17, 35). Notably, an unfavorable enthalpic contribution has also been observed for complex coacervation (10, 36, 37), indicating that the driving forces for phase separation of polyelectrolytes and for the formation of the ProTα-H1 dimer are closely related. The origin of the entropically dominated driving force of ProTα-H1 binding thus deserves closer investigation.

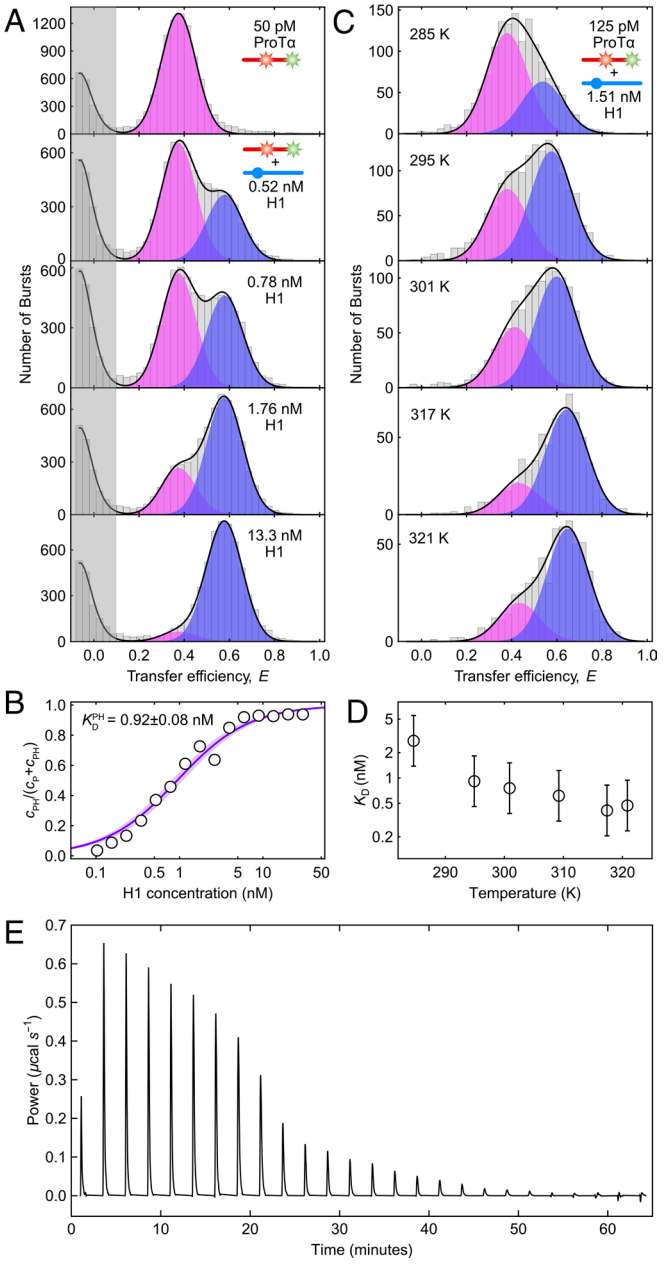

Fig. 1. The high-affinity binding between H1 and ProTα is endothermic. (*A*) Transfer efficiency histograms of 50 pM ProTα E56C/D110C labeled with Alexa Fluors 488 and 594 in the presence of increasing concentrations of unlabeled H1 (see the legend) at 208 mM monovalent salt concentration, globally fit with two Gaussian peak functions for the unbound (magenta) and bound (blue) ProTα populations, respectively (sum: black lines). (*B*) Representative example showing the bound fraction of labeled ProTα as a function of the H1 concentration fitted with a binding isotherm (solid line), in this case yielding an equilibrium dissociation constant of K_D = 0.92 ± 0.08 nM (shaded band: 90% CI). (*C*) Transfer efficiency histograms of 125 pM ProTα E56C/D110C labeled with Alexa Fluor 488/594 in the presence of 1.51 nM unlabeled H1 at 208 mM monovalent salt concentration, measured at different temperatures and fitted with two Gaussian peak functions for the unbound (magenta) and bound (blue) ProTα populations, respectively (sum: black lines). (*D*) The resulting temperature-dependent K_D shows rising affinity with increasing temperature, thus endothermic binding. Error bars represent a conservative systematic error of a factor of 2 on K_D (*SI Appendix*). (*E*) ITC thermogram, showing differential power as a function of time upon titrating ProTα into H1 at 208 mM monovalent salt concentration, which confirms endothermic binding.

Counterion Release Entropy Is a Strong Driving Force for ProTα-H1 Binding. Naively, it might be tempting to envision the driving force for binding between oppositely charged macromolecules in terms of simple Coulomb attraction between them. However, in this case, the process should be exothermic, in contrast to what we observe

*The association of polyelectrolytes with oppositely charged macromolecules is loosely referred to as polyelectrolyte complexation in the literature (9, 19, 21, 22, 24–27), which is commonly used as an overarching term that refers to the formation of small oligomers (9, 12, 13, 46)—especially dimers (soluble complexes)—but also dense liquid phases (coacervates) (36, 85, 108–110), kinetically arrested states, such as layered structures (111, 112), and almost solid-like materials (41, 113–117) that can exhibit dynamical transitions (59, 118, 119) (nonequilibrium complexes).

†Unless otherwise mentioned, we used KCl to vary the salt concentration in the presence of a fixed concentration of 10 mM Tris buffer. "Monovalent salt concentration" represents the contributions of both components, i.e., the fixed concentration of ionized Tris–HCl (8 mM) and the concentration of KCl (see *Material and Methods* for details).

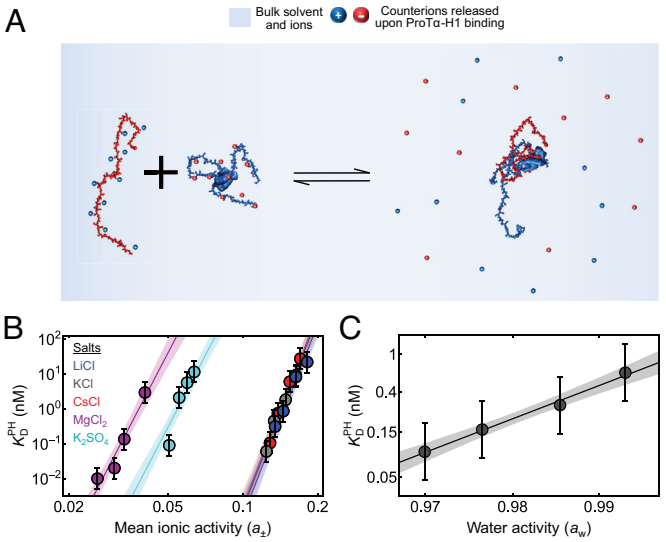

Fig. 2. Effects of ion and water activities on ProTα-H1 binding. (*A*) Schematic of ProTα binding to H1 associated with counterion release. (*B*) Equilibrium dissociation constant for ProTα-H1 binding, K_D^{PH}, at different mean ionic activities ($a_\pm$) of various salts (see the legend for color code). The data are fitted globally to obtain the number of monovalent and/or divalent ions released upon ProTα-H1 complex formation (see *SI Appendix* for details). The solid lines represent the fit, and the shaded regions represent 90% CIs. (*C*) K_D^{PH} at 208 mM monovalent salt concentration as a function of water activity (a_w), varied by changing the concentration of the osmolyte triethylene glycol (*SI Appendix*). The solid line represents a fit with Eq. **4** for estimating the apparent number of water molecules released upon ProTα-H1 complex formation (shaded band: 90% CI). All error bars represent a conservative systematic error of a factor of 2 on K_D (*SI Appendix*).

for H1 and ProTα. This simple picture ignores the essential role of counterions, present in the solution to ensure electroneutrality, and some of which associate with polyelectrolytes due to Coulomb attraction (19, 24). The presence of ions can extensively modulate biomolecular conformations, dynamics, and recognition (38–40), but the effects become particularly pertinent when two polyelectrolyte chains associate (be they biological or synthetic): Counterions are released into solution as charge interactions form between the chains, which results in a gain in translational entropy owing to the dilution of the ions into the bulk solution (Fig. 2*A*). This favorable counterion release entropy has been suggested to be a key driving force for polyelectrolyte complexation (24, 41–43). To quantify the contribution of counterions, Record and Lohman (24) developed an approach based on the principles of coupled equilibria between biomolecular binding and counterion release. In our case, unbound ProTα and H1 are associated with their counterions to attain charge neutrality; upon H1 binding to ProTα, n_- of the previously associated monovalent anions (A^-) and n_+ of the monovalent cations (C^+) are released:

$$\text{ProT}\alpha + \text{H1} \rightleftharpoons \text{ProT}\alpha\text{-H1} + n_+C^+ + n_-A^-. \quad [1]$$

However, n_+ and n_- can usually not be observed directly. Instead, we probe the apparent equilibrium

$$\text{ProT}\alpha + \text{H1} \overset{K_D^{PH}}{\rightleftharpoons} \text{ProT}\alpha\text{-H1}. \quad [2]$$

Record and Lohman (24) related the dependence of the corresponding observed equilibrium dissociation constant, K_D^{PH}, on the mean ionic activity of the participating ions, $a_\pm$, to the total number of counterions released, Δn:

$$\Delta n = n_+ + n_- \approx \frac{d\log K_D^{PH}}{d\log a_\pm}. \quad [3]$$

For H1 binding to ProTα, this dependence on salt concentration is remarkably strong: K_D^{PH} increases by six orders of magnitude (from $2.1^{+1.1}_{-0.8}$ pM to 4 ± 2 μM) between 165 mM and 340 mM monovalent salt (13, 28). Eq. **3** yields a release of 18 ± 1 monovalent counterions upon complex formation (13, 28), an unusually large number compared to other biomolecular systems (24, 44).

To assess the effect of the chemical identity of the counterions and their charge on the process, we extended this analysis to other chloride salts of monovalent cations (LiCl and CsCl) as well as divalent cations and anions [$K_2(SO_4)$ ad $MgCl_2$] (Fig. 2*B*). Effects of ions on polyelectrolyte complexation and biomolecular recognition can be complex, including the coupling of ion-specific conformational transitions to binding (45), differential ion uptake and release (46), and the ion-driven modulation of hydration effects (47). In the simplest scenario, however, the total number of anionic and cationic charges that are released upon binding to warrant charge neutrality is independent of the valence and identity of the counterions—this indeed seems to be the case for the binding of ProTα to H1: For the monovalent salts tested, the results are independent of chemical identity (Fig. 2*B*), suggesting that their interactions with the protein are nonspecific. For the divalent salts, the total number of released ions should be lower than for monovalent salts. Indeed, we observe a reduced slope for the dependence of log K_D^{PH} vs. log $a_\pm$ for salts with divalent cations or anions (Fig. 2*B*). From a global fit of the dependencies of K_D^{PH} on mean ionic activity for all five salts with a generalization of Eq. **3** (*SI Appendix*), we obtain 18 ± 1 for the sum of positive and negative charges released upon binding (Fig. 2*B*), respectively, consistent with our previous estimate of 18 ± 1 monovalent counterions released (13, 28). A general caveat of this analysis lies in the assumption that the extent of counterion adsorption is independent of salt concentration (24), which may not be fully realistic for flexible polyelectrolytes (48). Nevertheless, we can conclude that a large number of counterions is released when H1 binds to ProTα, and the resulting gain in their translational entropy is a driving force of complex formation (24, 41, 42).

Another contribution to binding processes originates from hydration (24, 49–51). These effects are more difficult to interpret mechanistically (52), but we assessed the role of water in ProTα-H1 complex formation by varying the water activity, a_w, with a neutral small-molecule osmolyte, triethylene glycol (53) (*SI Appendix*), and measuring its influence on K_D^{PH}. Formally, this result can be expressed in terms of the number of water molecules released upon complex formation, Δn_w, according to (51, 53)

$$\Delta n_w \approx \frac{d\log K_D^{PH}}{d\log a_w}, \quad [4]$$

yielding Δn_w = 80 ± 5 (Fig. 2*C*). For comparison, for folded proteins binding specifically to their cognate double-stranded DNA targets, Δn_w is considerably larger, typically with hundreds and up to ~1,000 water molecules released upon complex formation (47, 53–55). The lower value of Δn_w for ProTα-H1 binding is not entirely surprising since the IDPs remain highly hydrated owing to the disordered nature of the complex (13). Relating Δn_w to simple thermodynamic quantities is complicated by the many degrees of freedom involved in hydration

processes (52), but the free energy gain from the entropy of dilution is expected to be low because of the high bulk concentration of water (~55.5 M).

A final contribution to consider is configurational entropy of the polypeptide chains, which can play an important thermodynamic role in binding reactions of IDPs, for instance, if they are coupled to folding (56). In the case of H1 and ProTα, however, both IDPs retain their disorder and chain dynamics in the bound state (13), and the chains undergo only a minor compaction (Fig. 1*A* and *SI Appendix*, Fig. S1). Other degrees of freedom may contribute (18) but are difficult to identify unequivocally and are likely to be model-dependent. Based on a simple Gaussian chain model and a compaction by 23% in terms of end-to-end distance for ProTα at 208 mM monovalent salt concentration (*SI Appendix*, Fig. S1), we estimate a total change in configurational free energy of ~0.5 k_BT upon binding, assuming similar compaction for both ProTα and H1; this contribution is negligible compared to the total free energy of binding of ~20 k_BT.

Altogether, we thus conclude that counterion release entropy is likely to be a strong thermodynamic driving force for PH formation, as for polyelectrolyte complexation of synthetic systems (24, 41, 42), whereas changes in chain entropy of the IDPs are negligible for such a highly disordered complex. Contributions from hydration to the free energy of binding are likely to be relevant (57) but difficult to dissect into enthalpic and entropic contributions experimentally.

Resolving Ternary Complex Formation at Higher Protein Concentrations. So far, we have focused on the dimerization equilibrium P + H ⇌ PH, which describes the interaction between H1 and ProTα at picomolar and low nanomolar protein concentrations in the physiological ionic-strength range (13, 28). However, several observations indicate the existence of larger oligomers. First, transfer efficiencies and hydrodynamic radii for ProTα-H1 complexes were found to exhibit a continuous and progressive shift at large excess of one of the binding partners (13). Second, the interaction kinetics of H1 and ProTα are protein concentration-dependent and deviate from two-state behavior at high nanomolar protein concentrations and above (28), a signature of the formation of ternary complexes, such as ProTα$_2$-H1 (PPH) and ProTα-H1$_2$ (PHH) (58). The presence of ternary complexes also explains the fast exchange between bound and unbound states when the reaction is probed at the micromolar concentrations required for NMR spectroscopy (28). Third, molecular simulations demonstrate that the disordered nature of the complex facilitates the formation of higher-order oligomers (13, 15, 28). To probe the properties of ternary complexes more directly, we reasoned that since the interactions are charge-driven, reducing the salt concentration should further increase the affinity and decrease the kinetic exchange rates for the ternary complexes and might thus enable the detection of ternary complexes at equilibrium.

The existence of species beyond monomers and dimers does indeed become obvious in single-molecule titration experiments at low salt and elevated concentrations of unlabeled protein as distinct subpopulations in the transfer efficiency histograms (Fig. 3 *A* and *B*). For instance, we mixed 10 nM unlabeled ProTα and H1 each at 62 mM monovalent salt concentration and doped it with 70 pM labeled P as a probe that partitions between all ProTα-containing species and reports on their equilibrium fractions (Fig. 3*A*). Initially, a single population corresponding to the ProTα-H1 dimer is observed. If P + H ⇌ PH was the only contributing process, adding excess unlabeled P would simply cause a decrease in the observed equilibrium fraction of PH and an increase in the fraction of P. Instead, the decrease in the fraction of PH is accompanied by the appearance of a separate population with a transfer efficiency between those of PH and P. This new population reaches its maximum at a P:H stoichiometry of ~2:1, as expected for the ternary complex PPH. Adding even higher excess of P decreases the fraction of PPH, concomitant with an increase in the fraction of unbound P. From the fractions of PH and PPH, we obtain $K_D^{PPH} = 0.7^{+0.7}_{-0.4}$ nM for the reaction PPH ⇌ PH + P (Fig. 3*C*).

Analogously, we can populate the ternary complex PHH in experiments with an excess of H1. Fig. 3*B* shows a titration starting from

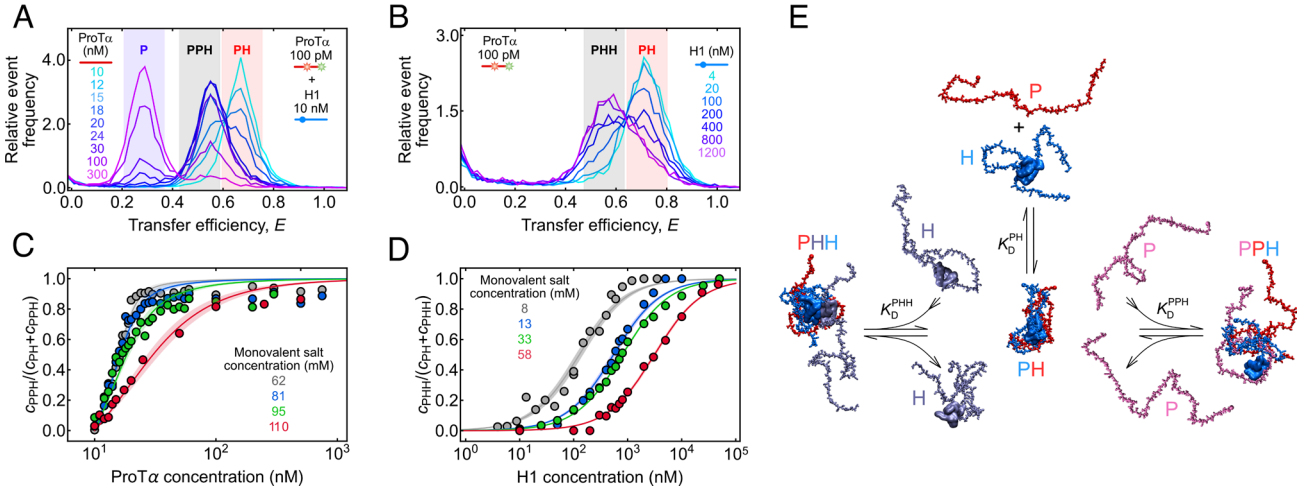

Fig. 3. Resolving ternary complexes with single-molecule spectroscopy at equilibrium. (*A*) Overlay of transfer efficiency histograms of 100 pM ProTα E56C/D110C labeled with Alexa Fluors 488/594 at 62 mM monovalent salt concentration in the presence of 10 nM unlabeled H1, with increasing concentrations of unlabeled ProTα (see legend), showing the formation of the PPH ternary complex as a separate peak. The red-, gray-, and purple-shaded regions indicate the peaks corresponding to PH, PPH, and unbound P, respectively. (*B*) Overlay of transfer efficiency histograms of 100 pM ProTα E56C/D110C labeled with Alexa Fluors 488/594 at 8 mM monovalent salt concentration, with increasing concentrations of unlabeled H1 (see legend), showing the formation of the PHH ternary complex as a separate peak. The red- and gray-shaded regions indicate the peaks corresponding to PH and PHH, respectively. (*C* and *D*) Fraction of ternary complexes, PPH (*C*) or PHH (*D*), as a function of unlabeled ProTα (*C*) or H1 concentration (*D*) at different monovalent salt concentrations (see legend) from the type of titrations shown in *A* and *B*. Solid lines represent fits with binding isotherms (*SI Appendix*); shaded regions indicate 90% CIs. (*E*) Schematic of ProTα (red, pink) and H1 (blue, purple) forming the PH dimer and PHH and PPH ternary complexes, using snapshots from coarse-grained simulations (59).

70 pM labeled ProTα saturated with 3 nM unlabeled H1 at a monovalent salt concentration of 8 mM (originating from the buffer alone), which results in a single population corresponding to the ProTα-H1 dimer. Upon adding more unlabeled H1, however, an additional population with lower transfer efficiency appears and increases with H1 concentration, corresponding to PHH. From the H1-dependent fraction of PHH, we obtain $K_D^{PHH} = 0.12^{+0.12}_{-0.06}$ μM for the reaction PHH ⇌ PH + H (Fig. 3*D*). These titration experiments thus not only allow us to resolve the ternary complexes PPH and PHH at equilibrium but also to quantify their stability.

With this approach, we can also probe the sensitivity of K_D^{PHH} and K_D^{PPH} to salt concentration and assess the role of counterion release for ternary complex formation (Fig. 4*A*). For both K_D^{PHH} and K_D^{PPH}, the highest experimentally accessible salt concentrations are limited by the decreasing separation between dimers and ternary complexes in the transfer efficiency histograms, which prevents assignment of the different species at high salt (Fig. 3 *A* and *B*); for K_D^{PPH}, the lowest accessible salt concentrations were limited by complex coacervation of ProTα and H1 occurring even at nanomolar protein concentrations (60). Nevertheless, extrapolating the salt concentration dependencies of K_D^{PH}, K_D^{PPH}, and K_D^{PHH} affords a systematic comparison of the free energies of formation for PH (ΔG^{PH}), PPH (ΔG^{PPH}), and PHH (ΔG^{PHH}). Across the experimentally accessible range, the absolute values of the free energies follow the order $|\Delta G^{PH}| > |\Delta G^{PPH}| > |\Delta G^{PHH}|$; i.e., PH is most stable, followed by PPH and PHH (Fig. 4*A*).

The slopes of the three salt concentration dependencies, however, are very different. Using Eq. **1**, we can estimate the numbers of counterions released upon formation of PPH and PHH,

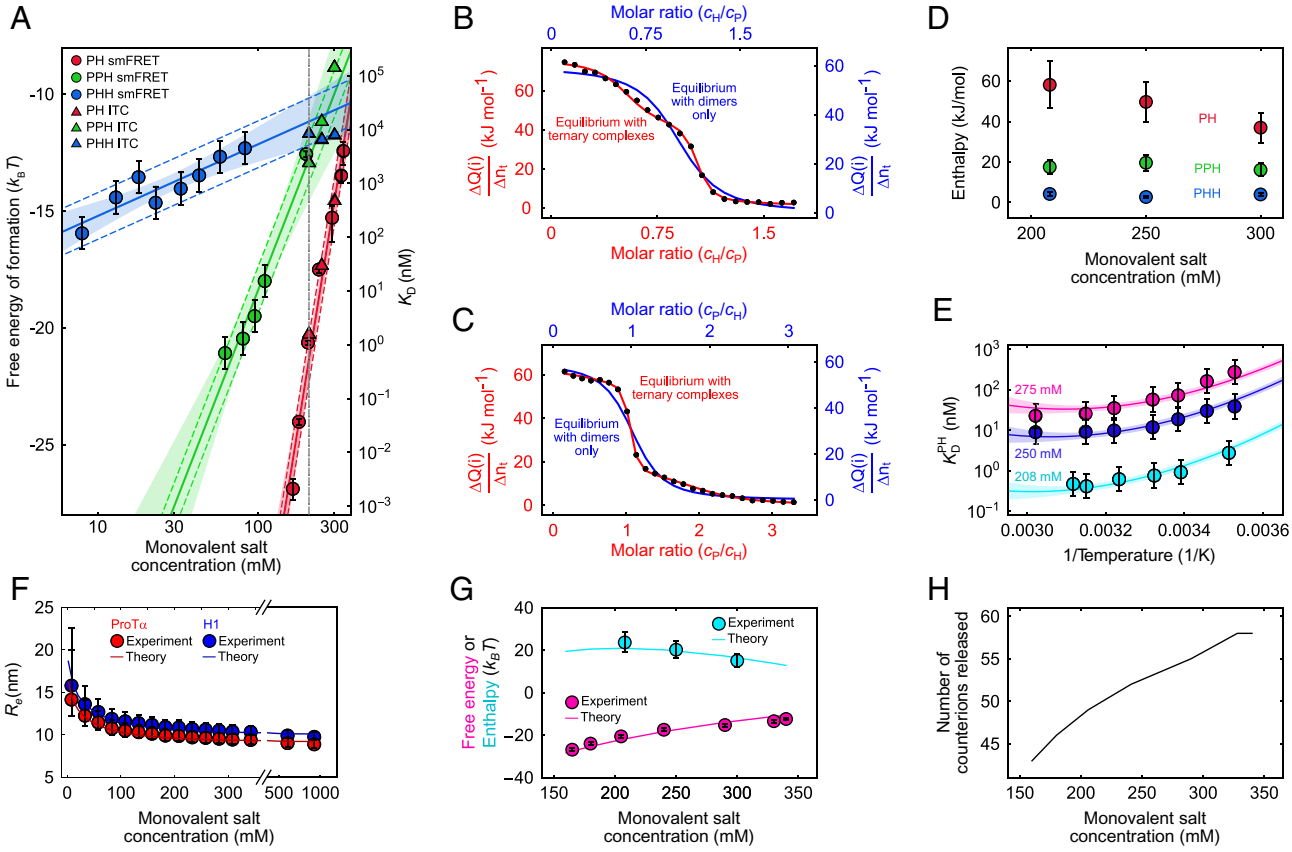

Fig. 4. Thermodynamics of ProTα-H1 binding including ternary complex formation. (*A*) Free energies and dissociation constants of forming PH dimers (red) and the ternary complexes PPH (green) and PHH (blue) from single-molecule FRET (circles; including previously published data (13, 59)) and ITC (triangles; see *SI Appendix*, Fig. S2, for titrations) as a function of monovalent salt concentration and fits with Eq. **3** (or analogous for PPH and PHH, solid lines; shaded bands: 90% CIs). Error bars on single-molecule data for PH are from Borgia et al. (13); for PHH and PPH, error bars represent a conservative systematic error of a factor of 2 on K_D (*SI Appendix*). Colored dashed lines represent ±1 k_BT from the fit lines, the upper bound estimated for the perturbation from dye labeling (59). The vertical dashed gray line indicates a monovalent salt concentration of 208 mM. (*B* and *C*) Integrated power from ITC per molar amount of injected titrant ($\Delta Q/\Delta n_t$; black points for each injection *i*) as a function of the molar ratio of both proteins, upon titrating H1 into ProTα (*B*) and ProTα into H1 (*C*) at 208 mM monovalent salt concentration. The data in (*B*) and (*C*) are globally fitted either with a 1:1 binding model (blue line and blue axis labels) or with a model including PHH and PPH ternary complexes (red line and axis labels) (see *SI Appendix* for details; note that the molar ratio is a fit parameter and thus slightly different for the two analyses). (*D*) Enthalpies of forming PH (red), PPH (green), and PHH (blue) from the ITC analysis (*B* and *C* and *SI Appendix*, Fig. S2) as a function of monovalent salt concentration. Error bars of ±20% are from the constraints on the protein concentrations used in fitting (*SI Appendix*, Table S2). (*E*) Temperature dependence of ProTα-H1 dissociation constants from single-molecule FRET measurements, shown as Van 't Hoff plots, at 208 mM (cyan), 250 mM (blue), and 275 mM (magenta) monovalent salt concentration. Error bars represent a conservative systematic error of a factor of 2 on K_D (*SI Appendix*). All three datasets are fitted globally with the integral form of the Van 't Hoff equation (solid lines; *SI Appendix*), with the heat capacity change upon binding as a shared fit parameter (*SI Appendix*; shaded bands: 90% CIs). (*F*) Salt dependence of the average end-to-end distance, R_e, for ProTα (red circles) and H1 (blue circles). R_e for ProTα was measured using single-molecule FRET; for H1, it is approximated using the scaling exponents for ProTα (see *SI Appendix* for details). Error bars are estimated from a conservative systematic error of ±0.03 on transfer efficiencies. The blue and red lines show R_e for ProTα and H1, respectively, using the theory for single isolated polyelectrolyte chains (see *SI Appendix* for details). (*G*) Comparison of the experimental free energy (magenta circles) and enthalpy (cyan circles) of ProTα-H1 complex formation as a function of monovalent salt concentration with those estimated from the theory of polyelectrolyte complexation (magenta and cyan lines for enthalpy and free energy, respectively; see *SI Appendix* for details). Error bars on experimental free energy and enthalpy as in (*A*) and (*D*). (*H*) The number of counterions released upon PH formation from the theory of polyelectrolyte complexation (see *SI Appendix* for details).

yielding values of 8 ± 1 and 1.3 ± 0.3, respectively (Fig. 4*A*), much lower than the value of 18 ± 1 for PH formation. Evidently, the largest charge compensation and counterion release occurs during formation of PH, corresponding to the largest driving force among the three complexes. The ProTα-H1 dimer has a nominal net charge of +9 owing to the higher net charge of H1 (+53) compared to ProTα (−44); adding another ProTα chain thus yields substantial further charge compensation and counterion release. In contrast, adding H1 to the dimer is electrostatically much less favorable and leads to little counterion release. Extrapolation to 208 mM monovalent salt concentration (Fig. 4*A*) yields values of the dissociation constants of $K_D^{PPH} = 3^{+14}_{-2}$ μM and $K_D^{PHH} = 13^{+26}_{-9}$ μM. The presence of ternary complexes[‡] must thus be taken into account for the quantitative interpretation of any experiment performed in the micromolar protein concentration range.

Quantifying Enthalpic Contributions in ProTα-H1 Complex Formation. Calorimetric measurements are considered the gold standard of thermodynamic analysis because they afford the direct measurement of binding enthalpies (61). However, since ITC cannot directly detect how many or which molecular species contribute, the accurate interpretation of the measured reaction heats requires an appropriate model comprising all equilibria involved. A semiempirical analysis of ITC measurements under conditions where both coacervation and soluble complex formation contribute have previously been used to infer positive enthalpies of ion pairing between polyelectrolytes (10, 36, 37). Here, we take the thermodynamic analysis one step further by performing measurements at sufficiently low protein concentrations so that phase separation does not contribute (60) and by explicitly accounting for the binding equilibria of dimers and ternary complexes of H1 and ProTα. Our detailed dissection of the ProTα-H1 interaction based on single-molecule FRET experiments over a wide range of protein and salt concentrations now allows us to approach such a complete thermodynamic analysis of ITC measurements. We performed ITC experiments at three different KCl concentrations corresponding to monovalent salt concentrations of 208 mM, 250 mM, and 300 mM, each with ProTα as a titrant (material injected) and H1 as a titrand (material in the sample cell) and vice versa (Fig. 4 *B* and *C* and *SI Appendix*, Fig. S2). Quantitative analysis of ITC measurements at lower salt concentrations was impeded by liquid–liquid phase separation (60).

The ITC titrations measured at 208 mM monovalent salt concentration, when fitted with a binding model involving only dimer formation, P + H ⇌ PH, yield apparent micromolar dissociation constants (34) (*SI Appendix*, Fig. S2 and Table S1) but show obvious deviations from the experimental data, reflecting the inadequacy of the model (Fig. 4 *B* and *C* and *SI Appendix*, Fig. S2). This result is not unexpected since the ITC measurements require micromolar protein concentrations, where both the dimer and the ternary complexes need to be considered. At 208 mM monovalent salt concentration, e.g., we expect that for 15 μM H1 and 45 μM ProTα, ~84% of the complexes are PPH. We thus include all three coupled equilibria, P + H ⇌ PH, PH + P ⇌ PPH, and PH + H ⇌ PHH, with their corresponding dissociation constants and reaction enthalpies K_D^{PH} and ΔH^{PH}, K_D^{PPH} and ΔH^{PPH}, and K_D^{PHH} and ΔH^{PHH}, respectively, as fit parameters, in a global analysis of the ITC measurements (see *SI Appendix* for details). We constrain the dissociation constants to be in agreement with the values extrapolated from the single-molecule data (binding free energies within ~1 k_BT, Fig. 4*A* and *SI Appendix*, Table S2) and obtain a good fit at all salt concentrations (Fig. 4 *A*–*C* and *SI Appendix*, Fig. S2). Taking into account ternary complex formation thus reconciles the apparent discrepancy between K_D^{PH} obtained from single-molecule FRET (13, 28) and ITC (34) (Fig. 4*A* and *SI Appendix*, Fig. S2).

Our ITC analysis yields positive values for ΔH^{PH}, ΔH^{PPH}, and ΔH^{PHH}; thus, not only dimerization but also ternary complex formation must be entropically driven. ΔH^{PH} is the largest among the three reaction enthalpies and decreases with monovalent salt concentration, from 58 ± 12 kJ mol^{-1} at 208 mM to 35 ± 7 kJ mol^{-1} at 300 mM (Fig. 4*D*). Electrostatic interactions, be they counterion accumulation near charged side chains of H1 and ProTα, or attraction between charged side chains in H1 and ProTα, are per se exothermic. However, if counterion condensation is more exothermic than the electrostatic attraction between the two IDPs, then the overall complex formation process can be endothermic. This hypothesis is compatible with the decrease in ΔH^{PH} with increasing salt concentration, where charge screening is expected to attenuate the exothermicity of the underlying microscopic processes. Additional contributions may originate from ion-water interactions (41). In summary, while counterion release entropy is a strong overall driving force for ProTα-H1 complex formation, the enthalpy of binding is likely to be determined by competing differential side chain–ion and side chain–side chain interactions.

To complete the thermodynamic characterization of ProTα-H1 binding, we extended our analysis to the temperature dependence of K_D^{PH} from the single-molecule FRET measurements at different salt concentrations (Figs. 1 *C* and *D* and 4*E*). The resulting Van 't Hoff plots show a small yet consistent curvature for all datasets, indicating a temperature dependence of ΔH^{PH} and the reaction entropy, ΔS^{PH}. The corresponding change in heat capacity upon binding, ΔC_p, can be obtained from a fit with the integrated form of the Van 't Hoff equation (*SI Appendix*). Using ΔH^{PH} from the ITC measurements[§], we fit all datasets with ΔC_p as a global fit parameter, yielding a value of −1.6 ± 0.3 kJ mol^{-1} K^{-1} (Fig. 4*E*). Identifying the molecular origins of ΔC_p is far from trivial, with potential contributions from different factors, including a differential temperature dependence of hydration for charged side chains and ions (62), but the small value of ΔC_p is typical of biomolecular binding and contrasts with the larger values associated with protein folding (63), where hydrophobic interactions are expected to make a larger contribution. The nonzero ΔC_p reflects some entropy–enthalpy compensation across different salt concentrations, resulting in a modest sensitivity of ΔG^{PH} to temperature, in contrast to the dramatic sensitivity of ΔG^{PH} to salt concentration. We can thus conclude that at the physiological temperature of 37 °C, PH complex formation is enthalpically unfavorable over a broad range of salt concentrations, up to ~350 mM, and counterion release is an important entropic driving force.

A Polymer Model of Polyelectrolyte Dimer Formation. We employed an analytical polyelectrolyte model incorporating counterion condensation and uniform expansion (64–66),

[‡]Note that we cannot exclude the population of higher oligomers in the presence of a large excess of binding partners if their transfer efficiencies are within experimental uncertainty of the ternary complexes. However, since K_D^{PPH} and K_D^{PHH} are orders of magnitude higher than K_D^{PH}, the analogous dissociation constants for higher-order complexes are likely to be much greater (28) and their contribution to the measurements correspondingly small. The dimerization of PH to dimers of dimers in the protein concentration range we use is incompatible with pulsed field gradient NMR and two-focus FCS measurements (13). We thus use the simplest model that consistently describes all experimental data.

[§]Either using ΔH^{PH} from ITC at 276 K (for 208 and 250 mM monovalent salt concentration) or estimated from a linear extrapolation of the measured ΔH^{PH} as a function of monovalent salt concentration (for 275 mM monovalent salt concentration, where ITC was not measured).

based on the Edwards–Muthukumar Hamiltonian (48, 67–69), to quantitatively describe the driving forces of the ProTα-H1 interaction. This theory of polyelectrolyte complexation takes into account conformational properties of the individual IDPs, IDP-associated counterions, and salt ions free in solution, resulting in various contributing free energy components: the translational entropy of IDP-associated and free counterions (referred to as F_1 and F_2, respectively, in *SI Appendix*); the electrostatic free energy due to the spatial correlations between free ions (F_3); the energy of ion-pairing for chain-counterion and interchain charge interactions (F_4); and the conformational free energy of the IDPs (F_5). For two complexing IDPs characterized by their respective degrees of polymerization and net charges (N_1, N_2, and N_{c1}, N_{c2}, respectively), intra- and interchain excluded-volume interaction strengths (w_0) as well as local dielectric mismatch parameters (δ_0 for chain-counterion and δ_{12} for chain–chain ion-pairing), the total free energy is self-consistently minimized with respect to chain dimensions and the number of adsorbed counterions, and this is done for different salt concentrations for the complexed state and the unbound states (64, 65) (see *SI Appendix* for details).

While free salt ions have an ideal-gas-like entropy in the system volume (F_2), bound counterions have substantially reduced translational entropy (F_1) since they are assumed to remain confined to a cylindrical volume along the chain contour. The electrostatic free energy among the free ions (F_3) is captured by a parametrically corrected Debye–Hückel theory using a multiplicative factor, Λ (see *SI Appendix*, Fig. S3 for details). There is a gain in ion-pairing energy (F_4) due to counterion condensation on the chains as well as from interchain ion-pairing. IDPs with charged segments contribute to the configurational entropy, excluded-volume interactions, and screened Coulomb interactions (F5). Upon chain complexation, counterions associated with the complexed parts of the chains are assumed to be released into the system volume, gaining translational entropy, while the dangling uncomplexed parts of the longer chain retain their adsorbed counterions.

Although the model takes into account the entropy and enthalpy of counterions and their interactions with the protein chains, and thus charge renormalization, it lacks an explicit description of charge patterning (18, 70) and charge regulation in terms of side chain pK_a shifts (71, 72), and it also uses a parametric correction for the free energy of ionic correlations instead of a formal description of this correlation energy (73) as a function of salt concentration. Charge regulation is likely to be negligible in the salt concentration range where we studied ProTα-H1 complex formation experimentally (see *SI Appendix* for details and *SI Appendix*, Fig. S4) (74, 75) and is therefore inconsequential for the interpretation of theoretical thermodynamic estimates; however, the estimates of the single-chain dimensions are slightly affected at low salt concentrations (see *SI Appendix* for details and *SI Appendix*, Fig. S4). The uniform net charge density assumed in the theory is likely to limit its applicability to highly charged polyelectrolytic sequences such as ProTα and H1. Hydration effects and solvent degrees of freedom (57, 62, 76) are beyond the scope of this type of theory. Nevertheless, the implicit solvent model of our approach accounts for some hydration effects in the enthalpic terms describing the protein–protein and protein–ion interactions, primarily by considering a local dielectric constant near the protein surface that can be different from the bulk, as supported by fluorescence spectroscopy with polarity-sensitive probes (77, 78); the theory approximates the distance dependence of the dielectric constant as a step function and assumes ion pairing to be represented by fixed dipoles as a simple approximation. Furthermore, the dielectric mismatch parameter serves as a single mean-field parameter that comprises two microscopic aspects of ion-pairing: a local dielectric constant and the effective dipole length, so it does not allow either parameter to be determined independently (see *SI Appendix* for details).

We parameterized the theory based on the experimental salt concentration-dependent observables—chain dimensions of ProTα and H1 and thermodynamic parameters for complex formation of ProTα-H1—using a sequential approach. An estimate of w_0 was obtained from the single-chain dimensions at high salt, where charge interactions are screened, and constraints on δ_0 were estimated based on the chain dimensions and their experimental uncertainty at low salt; subsequently, using the estimated value of w_0, we fitted the experimental thermodynamic observables (enthalpy and free energy of complexation) by systematically varying δ_0 (within the constraints from the previous step), δ_{12}, and Λ (see *SI Appendix* for details).

The resulting polymer model captures the thermodynamics of complex formation, both in terms of the reaction enthalpy and free energy for different salt concentrations (Fig. 4*G*), as well as the salt concentration-dependent chain dimensions (Fig. 4*F*) with only four adjustable parameters, w_0, δ_0, δ_{12}, and Λ. In line with our simple estimate for a Gaussian chain above, the change in configurational entropy of the chains upon binding (ΔF_5, *SI Appendix*, Fig. S3) makes a negligible contribution to the total free energy. The total enthalpy is determined by the balance between the Coulomb energy of ion-pair formation (F_4) and the enthalpic part of the free energy from correlations between free ions (F_3). With increasing salt concentration, more counterions are released upon IDP complex formation (Fig. 4*H*), but the decreasing entropy gain of each released ion owing to the larger bulk salt concentration compensates this effect and moderates the overall entropic driving force from counterion release at high salt (*SI Appendix*, Fig. S3). The decrease in enthalpy as a function of salt concentration resulting from the reduction in the number of bound ion pairs is offset by the increase in energy gain from more pronounced correlations between the free ions at higher salt concentrations (*SI Appendix*, Fig. S3). By considering the effect of the local dielectric environment on the electrostatic energy of ion pair formation, it becomes apparent that the entropy gain from the released counterions (ΔF_2) is the primary thermodynamic driving force (*SI Appendix*, Fig. S3).

Discussion

Most high-affinity protein complexes involve enthalpic and entropic contributions that are both favorable (17, 35). The high-affinity disordered complex between H1 and ProTα stands in contrast to this behavior: Its binding is entropically driven, with a large unfavorable enthalpy of similar magnitude as the total free energy of complex formation. Our results suggest that counterion-release entropy is a strong driving force for PH complex formation. This finding highlights the importance of counterions in interactions involving highly charged biomacromolecules and leads to behavior such as increasing affinity with temperature (Figs. 1*C* and 4*E*). Polyelectrolyte interactions of this kind abound in the cell, especially in the nucleus, where charged IDPs and nucleic acids are key players in chromatin structure and transcriptional regulation (15, 28, 79–81).

Much of the behavior we observe here for H1 and ProTα is reminiscent of synthetic polyelectrolytes (36, 37, 41, 42, 82), especially the important role of counterion release entropy (42, 82) and the endothermic character of the interaction (36, 37). However, a key aspect of our results is that we unambiguously detect and quantify the presence of stoichiometrically defined soluble complexes between H1 and ProTα—the PH dimer and the two ternary

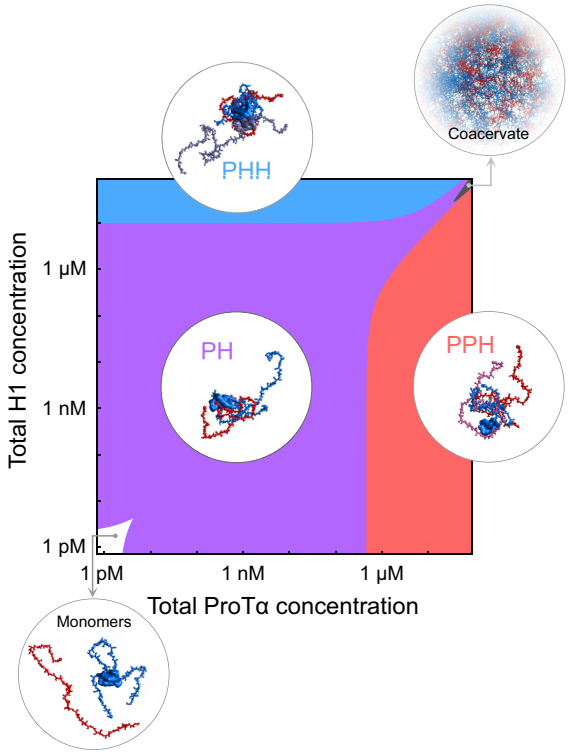

Fig. 5. Diagram of assembly states formed by H1 and ProTα as a function of protein concentrations at 165 mM monovalent salt. The colored regions indicate the predominant oligomeric species. If both protein concentrations are in the low picomolar range or below (white area), ProTα and H1 are predominantly monomeric. In the purple, blue, and red regions, ProTα-H1 (PH), ProTα-H1$_2$ (PHH), and ProTα$_2$-H1 (PPH) are the predominant oligomeric species, respectively. The dark gray region at high concentrations of both proteins indicates conditions where phase separation by complex coacervation occurs (57). Note that the reentrant boundaries for complex coacervation are approximate. The other regions are calculated based on the equilibrium dissociation constants K_D^{PH}, K_D^{PPH}, and K_D^{PHH} at 165 mM salt (*SI Appendix*, Eqs. **S1**–**S3**). Snapshots of complexes and the dense phase are based on simulations (13, 59).

complexes PPH and PHH—afforded by the ability of single-molecule spectroscopy to identify different molecular species as distinct subpopulations (29–32). Only at near charge-balanced stoichiometry and above tens of micromolar protein concentrations does phase separation set in at physiological salt concentrations (Fig. 5) (60). For synthetic polyelectrolytes, as well as some biomolecular systems such as gelatin, indications for the presence of soluble complexes from experiments have been reported (36, 37, 83, 84), but the unambiguous detection and characterization of species such as dimeric and trimeric complexes has remained elusive, presumably owing to the low critical concentrations for the coacervation of binary mixtures of oppositely charged polyelectrolytes (21, 85) and the lack of experimental methods required for investigating the ultralow polyelectrolyte concentrations where the association equilibria for the formation of dimers and ternary complexes can be probed. Correspondingly, the formation of well-defined oligomeric polyelectrolyte complexes has primarily been investigated via simulations and theory (42, 57, 64, 65, 82, 86), and small soluble complexes such as dimers have been postulated to be a first step of polyelectrolyte complexation preceding coacervation (37, 83, 84, 87). Considering the obvious parallels between highly charged IDPs and synthetic polyelectrolytes, the dimers and ternary complexes of ProTα and H1 are thus likely to resemble the small soluble complexes of synthetic polyelectrolytes. Our single-molecule approach is expected to be extendable to synthetic polyelectrolytes and would facilitate their quantitative investigation, including their mechanistic role in coacervation.

Another parallel to the behavior of synthetic polyelectrolytes is the thermodynamic signature we observe for the formation of ProTα-H1 oligomers, especially its endothermicity, which requires a pronounced entropic driving force to yield a strong interaction. A positive interaction enthalpy has previously been reported for synthetic polyelectrolytes, but the need to separate the contributions of small oligomers from coacervation complicates quantitative modeling (36, 37). Here, we demonstrate that such modeling is feasible for H1 and ProTα since phase separation is absent under our experimental conditions, and independent information on the stabilities and thus concentrations of the contributing dimer and ternary complexes is available from single-molecule measurements. Obviously, both the dimer and the ternary complexes need to be accounted for in the quantitative analysis of binding experiments at micromolar protein concentrations, where they are substantially populated at physiologically relevant salt concentrations. This insight resolves the orders-of-magnitude discrepancy between the affinity of the PH complex obtained from single-molecule experiments and the apparent affinities inferred from ITC if an inadequate model involving only dimer formation is assumed (34). Ternary complex formation also reconciles the fast exchange between bound and unbound states observed in NMR experiments at high micromolar concentrations with the high affinity of ProTα-H1 complex formation (28). The underlying mechanism of competitive substitution (88) may also be involved in transcriptional regulation (15).

We rationalize our results with concepts from the field of synthetic polyelectrolytes (13, 28, 31, 36, 37, 42, 64, 65, 82, 83, 87), in particular a minimal mean-field theory that treats a salt-moderated balance between Coulomb energy of bound ion pairs and free-ion entropy, and accounts for counterion adsorption and release (64, 65). Recent theoretical considerations based on the temperature dependence of the relative permittivity of bulk water suggest the relevance of solvent entropy for polyelectrolyte interactions related to the reorientational entropy of the dipolar solvent associated with ion-pair formation (57). Our theoretical approach indicates substantial counterion condensation on the chains, potentially amplified by a reduced dielectric constant near the polypeptide chain (48, 89, 90), which is expected to render solvent orientation effects small compared to the entropy gain from counterion release. One way of testing and refining the parameters used in the current theoretical framework might be all-atom molecular dynamics simulations (60, 62, 91). The modular nature of the theory would in principle also allow aspects such as charge patterning and charge regulation (92, 93) to be incorporated explicitly.

Our results may further contribute to a quantitative understanding of polyelectrolyte complex coacervation by complementing theories for phase separation that explicitly account for polyelectrolyte-associated counterions (36, 94–96) but do not yet account for the diversity of soluble complexes in the dilute phase. From the perspective of kinetics (97), the formation of small oligomers or clusters may be the earliest steps of phase separation, and for subsaturated solutions of several RNA-binding proteins that undergo homotypic phase separation, a heterogeneous distribution of clusters ranging from tens or hundreds of molecules to mesoscale assemblies has been observed (98). A continuum of such assemblies may thus provide a link between the small oligomers we observe here and phase separation. However, in contrast to homotypic cluster formation, in heterotypic systems such as ProTα and H1, not only the absolute but also the relative concentrations are crucial for cluster formation. In such systems, higher-order oligomers may define the phase boundaries, particularly for reentrant phase separation (99). It will be an interesting topic of future research whether an analogous broad range of heterotypic oligomers and clusters exists for systems like H1 and ProTα that undergo complex coacervation.

With counterion release entropy as a principle driving force for polyelectrolyte complex formation, the affinity between chains can potentially become extremely large since the number of counterions adsorbed on a polyelectrolyte chain increases with the number of charged groups and thus the degree of polymerization (48, 64, 66). The cellular milieu is rife with highly charged flexible biopolymers, such as nucleic acids (100), inorganic polyphosphate (101), and highly charged IDPs (13), and high-affinity interactions as well as complex coacervation can result without the need for interactions encoded by folded domains. Considering the combinatorial possibilities of complexes that can arise from such polyelectrolyte molecules in a cell, an obvious question is the origin of specificity in such interactions. Specificity can arise from distinct patterns of spatial and temporal localizations and concentrations of interaction partners such that the likelihood of a specific pair of such molecules forming a complex is maximized. Other regulatory processes, such as posttranslational modifications, to which IDPs are particularly amenable, as well as patterning of charged residues, can also contribute (18, 102, 103). Polyelectrolyte interactions are likely to often act in synergy with structured domains and motifs, a combination that is widespread in nucleic acid-binding proteins (104). Polyelectrolyte interactions and counterion release as a driving force are thus likely to be of general importance for biomolecular interactions (19, 24, 51, 105), and understanding the underlying mechanisms will be essential for quantifying intracellular communication.

Material and Methods

Proteins were recombinantly expressed in *Escherichia coli*, purified, and labeled for single-molecule FRET experiments as described previously (13, 28, 77). The details of single-molecule experiments and the experimental setup have been described before (13, 28, 106). Calorimetry experiments were performed on a MicroCal iTC200 calorimeter. See *SI Appendix* for detailed descriptions on protein expression, purification, labeling, single-molecule FRET, and calorimetry experiments and analysis, and a description of the theory.

Data, Materials, and Software Availability. Code for analysis of single-molecule and computational data has been deposited in GitHub (https://github.com/SchulerLab/Fretica.git) (107). All other data are included in the manuscript and/or supporting information.

ACKNOWLEDGMENTS. We thank Olga Bozovich and Ilian Jelezarov for help with ITC experiments and analysis, Hagen Hofmann, and Andrea Soranno for helpful discussions, Robert Best for structural representations from coarse-grained simulations, Edward Lemke for providing the pBAD-Int-CBD-12His plasmid, Janine van Uffelen for technical assistance, and Janneke Hille Ris Lambers and Annette Bieger Altermatt for access to vapor pressure osmometry. We thank the Functional Genomics Center Zurich, especially Dr. Serge Chesnov, for excellent mass spectrometry service. This work was supported by the Swiss National Science Foundation (B.S.), the Novo Nordisk Foundation Challenge program REPIN (#NNF18OC0033926, B.S.), the European Union's Horizon 2020 research and innovation programme under the Marie Skłodowska-Curie grant agreement ID 898228 (A.C.), the Forschungskredit of the University of Zurich (A.C. and N.G.), and the Ministry of Education, Government of India (S.G., S.M., and A.K.).

Author affiliations: [a]Department of Biochemistry, University of Zurich, Zurich 8057, Switzerland; [b]Department of Physical Sciences and Centre for Advanced Functional Materials, Indian Institute of Science Education and Research Kolkata, Mohanpur 741246, India; and [c]Department of Physics, University of Zurich, Zurich 8057, Switzerland

Author contributions: A.C., A.K., and B.S. designed research; A.C., A.B., S.G., A.S., S.M., R.S.E., M.B.B., N.G., and M.T.I. performed research; A.C., A.S., M.B.B., T.Y., P.Ł., R.Z., and D.N. contributed new reagents/analytic tools; A.C., S.G., S.M., and D.N. analyzed data; A.C., A.K. and B.S. wrote the paper with inputs from all authors; and A.K. and B.S. supervised research.

1. V. Csizmok, A. V. Follis, R. W. Kriwacki, J. D. Forman-Kay, Dynamic protein interaction networks and new structural paradigms in signaling. *Chem. Rev.* **116**, 6424–6462 (2016).
2. R. B. Berlow, H. J. Dyson, P. E. Wright, Functional advantages of dynamic protein disorder. *FEBS Lett.* **589**, 2433–2440 (2015).
3. A. K. Dunker, M. S. Cortese, P. Romero, L. M. Iakoucheva, V. N. Uversky, Flexible nets. The roles of intrinsic disorder in protein interaction networks. *FEBS J.* **272**, 5129–5148 (2005).
4. P. E. Wright, H. J. Dyson, Linking folding and binding. *Curr. Opin. Struct. Biol.* **19**, 31–38 (2009).
5. P. Tompa, M. Fuxreiter, Fuzzy complexes: Polymorphism and structural disorder in protein–protein interactions. *Trends Biochem. Sci.* **33**, 2–8 (2008).
6. T. Mittag, L. E. Kay, J. D. Forman-Kay, Protein dynamics and conformational disorder in molecular recognition. *J. Mol. Recognit.* **23**, 105–116 (2010).
7. T. Mittag *et al.*, Dynamic equilibrium engagement of a polyvalent ligand with a single-site receptor. *Proc. Natl. Acad. Sci. U.S.A.* **105**, 17772–17777 (2008).
8. S. Milles *et al.*, Plasticity of an ultrafast interaction between nucleoporins and nuclear transport receptors. *Cell* **163**, 734–745 (2015).
9. B. Schuler *et al.*, Binding without folding–the biomolecular function of disordered polyelectrolyte complexes. *Curr. Opin. Struct. Biol.* **60**, 66–76 (2020).
10. A. L. Turner *et al.*, Highly disordered histone H1-DNA model complexes and their condensates. *Proc. Natl. Acad. Sci. U.S.A.* **115**, 11964–11969 (2018).
11. N. Danilenko *et al.*, Histone chaperone exploits intrinsic disorder to switch acetylation specificity. *Nat. Commun.* **10**, 3435 (2019).
12. E. D. Holmstrom, Z. Liu, D. Nettels, R. B. Best, B. Schuler, Disordered RNA chaperones can enhance nucleic acid folding via local charge screening. *Nat. Commun.* **10**, 2453 (2019).
13. A. Borgia *et al.*, Extreme disorder in an ultrahigh-affinity protein complex. *Nature* **555**, 61–66 (2018).
14. E. M. George, D. T. Brown, Prothymosin α is a component of a linker histone chaperone. *FEBS Lett.* **584**, 2833–2836 (2010).
15. P. O. Heidarsson *et al.*, Release of linker histone from the nucleosome driven by polyelectrolyte competition with a disordered protein. *Nat. Chem.* **14**, 224–231 (2022).
16. S. L. Shammas, J. M. Rogers, S. A. Hill, J. Clarke, Slow, reversible, coupled folding and binding of the spectrin tetramerization domain. *Biophys. J.* **103**, 2203–2214 (2012).
17. W. E. Stites, Protein−protein interactions: Interface structure, binding thermodynamics, and mutational analysis. *Chem. Rev.* **97**, 1233–1250 (1997).
18. M. K. Hazra, Y. Levy, Affinity of disordered protein complexes is modulated by entropy–energy reinforcement. *Proc. Natl. Acad. Sci. U.S.A.* **119**, e2120456119 (2022).
19. M. Muthukumar, 50th anniversary perspective: A perspective on polyelectrolyte solutions. *Macromolecules* **50**, 9528–9560 (2017).
20. J. van der Gucht, E. Spruijt, M. Lemmers, M. A. Cohen Stuart, Polyelectrolyte complexes: Bulk phases and colloidal systems. *J. Colloid Interface Sci.* **361**, 407–422 (2011).
21. S. Srivastava, M. V. Tirrell, Polyelectrolyte complexation. *Adv. Chem. Phys.* **161**, 499–544 (2016).
22. V. A. Kabanov, Polyelectrolyte complexes in solution and in bulk. *Russ. Chem. Rev.* **74**, 3–20 (2005).
23. A. M. Rumyantsev, N. E. Jackson, J. J. de Pablo, Polyelectrolyte complex coacervates: Recent developments and new frontiers. *Annu. Rev. Condens. Matter Phys.* **12**, 155–176 (2021).
24. M. T. Record Jr., C. F. Anderson, T. M. Lohman, Thermodynamic analysis of ion effects on the binding and conformational equilibria of proteins and nucleic acids: The roles of ion association or release, screening, and ion effects on water activity. *Q. Rev. Biophys.* **11**, 103–178 (1978).
25. C. E. Sing, Development of the modern theory of polymeric complex coacervation. *Adv. Colloid Interface Sci.* **239**, 2–16 (2017).
26. K. Achazi *et al.*, Understanding the interaction of polyelectrolyte architectures with proteins and biosystems. *Angew. Chem. Int. Ed. Engl.* **60**, 3882–3904 (2021).
27. C. L. Cooper, P. L. Dubin, A. B. Kayitmazer, S. Turksen, Polyelectrolyte–protein complexes. *Curr. Opin. Colloid Interface Sci.* **10**, 52–78 (2005).
28. A. Sottini *et al.*, Polyelectrolyte interactions enable rapid association and dissociation in high-affinity disordered protein complexes. *Nat. Commun.* **11**, 5736 (2020).
29. A. C. Ferreon, C. R. Moran, Y. Gambin, A. A. Deniz, Single-molecule fluorescence studies of intrinsically disordered proteins. *Methods Enzymol.* **472**, 179–204 (2010).
30. L. A. Metskas, E. Rhoades, Single-molecule FRET of intrinsically disordered proteins. *Annu. Rev. Phys. Chem.* **71**, 391–414 (2020).
31. A. Chowdhury, D. Nettels, B. Schuler, Interaction dynamics of intrinsically disordered proteins from single-molecule spectroscopy. *Annu. Rev. Biophys.* **52**, 433–462 (2023).
32. H. Mazal, G. Haran, Single-molecule FRET methods to study the dynamics of proteins at work. *Curr. Opin. Biomed. Eng.* **12**, 8–17 (2019).
33. E. Sisamakis, A. Valeri, S. Kalinin, P. J. Rothwell, C. A. M. Seidel, Accurate single-molecule FRET studies using multiparameter fluorescence detection. *Methods Enzymol.* **475**, 455–514 (2010).
34. H. Feng, B. R. Zhou, Y. Bai, Binding affinity and function of the extremely disordered protein complex containing human linker histone H1.0 and its chaperone protalpha. *Biochemistry* **57**, 6645–6648 (2018).
35. J. A. Caro *et al.*, Entropy in molecular recognition by proteins. *Proc. Natl. Acad. Sci. U.S.A.* **114**, 6563 (2017).
36. L.-W. Chang *et al.*, Sequence and entropy-based control of complex coacervates. *Nat. Commun.* **8**, 1273 (2017).
37. D. Priftis, N. Laugel, M. Tirrell, Thermodynamic characterization of polypeptide complex coacervation. *Langmuir* **28**, 15947–15957 (2012).
38. B. I. M. Wicky, S. L. Shammas, J. Clarke, Affinity of IDPs to their targets is modulated by ion-specific changes in kinetics and residual structure. *Proc. Natl. Acad. Sci. U.S.A.* **114**, 9882–9887 (2017).
39. S. Müller-Späth *et al.*, Charge interactions can dominate the dimensions of intrinsically disordered proteins. *Proc. Natl. Acad. Sci. U.S.A.* **107**, 14609–14614 (2010).
40. J. Lipfert, S. Doniach, R. Das, D. Herschlag, Understanding nucleic acid–ion interactions. *Annu. Rev. Biochem.* **83**, 813–841 (2014).
41. J. Fu, J. B. Schlenoff, Driving forces for oppositely charged polyion association in aqueous solutions: Enthalpic, entropic, but not electrostatic. *J. Am. Chem. Soc.* **138**, 980–990 (2016).
42. Z. Ou, M. Muthukumar, Entropy and enthalpy of polyelectrolyte complexation: Langevin dynamics simulations. *J. Chem. Phys.* **124**, 154902 (2006).

43. G. S. Manning, J. Ray, Counterion condensation revisited. *J. Biomol. Struct. Dyn.* **16**, 461–476 (1998).
44. R. Vancraenenbroeck, Y. S. Harel, W. Zheng, H. Hofmann, Polymer effects modulate binding affinities in disordered proteins. *Proc. Natl. Acad. Sci. U.S.A.* **116**, 19506–19512 (2019).
45. A. G. Kozlov, T. M. Lohman, Effects of monovalent anions on a temperature-dependent heat capacity change for Escherichia coli SSB tetramer binding to single-stranded DNA. *Biochemistry* **45**, 5190–5205 (2006).
46. L. B. Overman, W. Bujalowski, T. M. Lohman, Equilibrium binding of Escherichia coli single-strand binding protein to single-stranded nucleic acids in the (SSB)65 binding mode. Cation and anion effects and polynucleotide specificity. *Biochemistry* **27**, 456–471 (1988).
47. K. A. Vander Meulen, R. M. Saecker, M. T. Record, Formation of a wrapped DNA–Protein interface: Experimental characterization and analysis of the large contributions of ions and water to the thermodynamics of binding IHF to H′ DNA. *J. Mol. Biol.* **377**, 9–27 (2008).
48. M. Muthukumar, Theory of counter-ion condensation on flexible polyelectrolytes: Adsorption mechanism. *J. Chem. Phys.* **120**, 9343–9350 (2004).
49. A. Tamura, P. L. Privalov, The entropy cost of protein association. *J. Mol. Biol.* **273**, 1048–1060 (1997).
50. P. L. Privalov, A. I. Dragan, C. Crane-Robinson, Interpreting protein/DNA interactions: Distinguishing specific from non-specific and electrostatic from non-electrostatic components. *Nucleic Acids Res.* **39**, 2483–2491 (2011).
51. M. T. Record Jr., W. Zhang, C. F. Anderson, Analysis of effects of salts and uncharged solutes on protein and nucleic acid equilibria and processes: A practical guide to recognizing and interpreting polyelectrolyte effects, Hofmeister effects, and osmotic effects of salts. *Adv. Protein Chem.* **51**, 281–353 (1998).
52. M. Heyden, Disassembling solvation free energies into local contributions-toward a microscopic understanding of solvation processes. *Wiley Interdiscip. Rev. Comput. Mol. Sci.* **9**, e1390 (2019).
53. M. M. Garner, D. C. Rau, Water release associated with specific binding of gal repressor. *EMBO J.* **14**, 1257–1263 (1995).
54. J.-H. Ha, M. W. Capp, M. D. Hohenwalter, M. Baskerville, M. T. Record, Thermodynamic stoichiometries of participation of water, cations and anions in specific and non-specific binding of lac repressor to DNA: Possible thermodynamic origins of the "glutamate effect" on protein-DNA interactions. *J. Mol. Biol.* **228**, 252–264 (1992).
55. M. G. Fried *et al.*, Role of hydration in the binding of lac repressor to DNA. *J. Biol. Chem.* **277**, 50676–50682 (2002).
56. F. F. Theisen *et al.*, Quantification of conformational entropy unravels effect of disordered flanking region in coupled folding and binding. *J. Am. Chem. Soc.* **143**, 14540–14550 (2021).
57. S. Chen, Z.-G. Wang, Driving force and pathway in polyelectrolyte complex coacervation. *Proc. Natl. Acad. Sci. U.S.A.* **119**, e2209975119 (2022).
58. T. Y. Chen, Y. S. Cheng, P. S. Huang, P. Chen, Facilitated unbinding via multivalency-enabled ternary complexes: New paradigm for protein-DNA interactions. *Acc. Chem. Res.* **51**, 860–868 (2018).
59. Y. Zhang *et al.*, Molecular origin of the glass transition in polyelectrolyte assemblies. *ACS Cent. Sci.* **4**, 638–644 (2018).
60. N. Galvanetto *et al.*, Extreme dynamics in a biomolecular condensate. *Nature* **619**, 876–883 (2023).
61. M. W. Freyer, E. A. Lewis, Isothermal titration calorimetry: Experimental design, data analysis, and probing macromolecule/ligand binding and kinetic interactions. *Methods Cell Biol.* **84**, 79–113 (2008).
62. M. J. Fossat, X. Zeng, R. V. Pappu, Uncovering differences in hydration free energies and structures for model compound mimics of charged side chains of amino acids. *J. Phys. Chem. B* **125**, 4148–4161 (2021).
63. A. Cooper, Heat capacity effects in protein folding and ligand binding: A re-evaluation of the role of water in biomolecular thermodynamics. *Biophys. Chem.* **115**, 89–97 (2005).
64. S. Ghosh, S. Mitra, A. Kundagrami, Polymer complexation: Partially ionizable asymmetric polyelectrolytes. *J. Chem. Phys.* **158**, 204903 (2023), 10.1063/1065.0147323.
65. S. Mitra, A. Kundagrami, Polyelectrolyte complexation of two oppositely charged symmetric polymers: A minimal theory. *J. Chem. Phys.* **158**, 014904 (2023).
66. A. Kundagrami, M. Muthukumar, Effective charge and coil—globule transition of a polyelectrolyte chain. *Macromolecules* **43**, 2574–2581 (2010).
67. S. F. Edwards, P. Singh, Size of a polymer molecule in solution. Part 1.–Excluded volume problem. *J. Chem. Soc. Faraday Trans.* **275**, 1001–1019 (1979).
68. M. Muthukumar, Adsorption of a polyelectrolyte chain to a charged surface. *J. Chem. Phys.* **86**, 7230–7235 (1987).
69. M. Muthukumar, *Physics of Charged Macromolecules: Synthetic and Biological Systems* (Cambridge University Press, Cambridge, 2023).
70. R. K. Das, R. V. Pappu, Conformations of intrinsically disordered proteins are influenced by linear sequence distributions of oppositely charged residues. *Proc. Natl. Acad. Sci. U.S.A.* **110**, 13392–13397 (2013).
71. M. A. S. Hass, F. A. A. Mulder, Contemporary NMR studies of protein electrostatics. *Annu. Rev. Biophys.* **44**, 53–75 (2015).
72. M. J. Fossat, A. E. Posey, R. V. Pappu, Quantifying charge state heterogeneity for proteins with multiple ionizable residues. *Biophys. J.* **120**, 5438–5453 (2021).
73. R. Kjellander, A multiple decay-length extension of the Debye-Hückel theory: To achieve high accuracy also for concentrated solutions and explain under-screening in dilute symmetric electrolytes. *Phys. Chem. Chem. Phys.* **22**, 23952–23985 (2020).
74. B. J. Payliss, J. Vogel, A. K. Mittermaier, Side chain electrostatic interactions and pH-dependent expansion of the intrinsically disordered, highly acidic carboxyl-terminus of γ-tubulin. *Protein Sci.* **28**, 1095–1105 (2019).
75. K. Tamiola, R. M. Scheek, P. van der Meulen, F. A. A. Mulder, pepKalc: Scalable and comprehensive calculation of electrostatic interactions in random coil polypeptides. *Bioinformatics* **34**, 2053–2060 (2018).
76. R. Wuttke *et al.*, Temperature-dependent solvation modulates the dimensions of disordered proteins. *Proc. Natl. Acad. Sci. U.S.A.* **111**, 5213–5218 (2014).
77. A. Chowdhury *et al.*, Mechanism-dependent modulation of ultrafast interfacial water dynamics in intrinsically disordered protein complexes. *Angew. Chem. Int. Ed. Engl.* **58**, 4720–4724 (2019).
78. E. Fischermeier *et al.*, Dipolar relaxation dynamics at the active site of an ATPase regulated by membrane lateral pressure. *Angew. Chem. Int. Ed. Engl.* **56**, 1269–1272 (2017).
79. B. Schuler *et al.*, Binding without folding–the biomolecular function of disordered polyelectrolyte complexes. *Curr. Opin. Struct. Biol.* **60**, 66–76 (2019).
80. C. F. Anderson, M. T. Record Jr., Salt-nucleic acid interactions. *Annu. Rev. Phys. Chem.* **46**, 657–700 (1995).
81. J. Liu *et al.*, Intrinsic disorder in transcription factors. *Biochemistry* **45**, 6873–6888 (2006).
82. V. S. Rathee, H. Sidky, B. J. Sikora, J. K. Whitmer, Role of associative charging in the entropy-energy balance of polyelectrolyte complexes. *J. Am. Chem. Soc.* **140**, 15319–15328 (2018).
83. L. Vitorazi *et al.*, Evidence of a two-step process and pathway dependency in the thermodynamics of poly(diallyldimethylammonium chloride)/poly(sodium acrylate) complexation. *Soft Matter.* **10**, 9496–9505 (2014).
84. A. Veis, A review of the early development of the thermodynamics of the complex coacervation phase separation. *Adv. Colloid Interface Sci.* **167**, 2–11 (2011).
85. E. Spruijt, A. H. Westphal, J. W. Borst, M. A. Cohen Stuart, J. van der Gucht, Binodal compositions of polyelectrolyte complexes. *Macromolecules* **43**, 6476–6484 (2010).
86. E. Meneses-Juárez, C. Márquez-Beltrán, J. F. Rivas-Silva, U. Pal, M. González-Melchor, The structure and interaction mechanism of a polyelectrolyte complex: A dissipative particle dynamics study. *Soft Matter* **11**, 5889–5897 (2015).
87. S. Chen, P. Zhang, Z.-G. Wang, Complexation between oppositely charged polyelectrolytes in dilute solution: Effects of charge asymmetry. *Macromolecules* **55**, 3898–3909 (2022).
88. B. Peng, M. Muthukumar, Modeling competitive substitution in a polyelectrolyte complex. *J. Chem. Phys.* **143**, 243133 (2015).
89. E. L. Mehler, G. Eichele, Electrostatic effects in water-accessible regions of proteins. *Biochemistry* **23**, 3887–3891 (1984).
90. G. Lamm, G. R. Pack, Calculation of dielectric constants near polyelectrolytes in solution. *J. Phys. Chem. B* **101**, 959–965 (1997).
91. G. M. Wadsworth *et al.*, RNAs undergo phase transitions with lower critical solution temperatures. bioRxiv [Preprint] (2022). https://doi.org/10.1101/2022.10.17.512593 (Accessed 14 September 2023).
92. L. Sawle, K. Ghosh, A theoretical method to compute sequence dependent configurational properties in charged polymers and proteins. *J. Chem. Phys.* **143**, 085101 (2015).
93. M. Ghasemi, R. G. Larson, Role of electrostatic interactions in charge regulation of weakly dissociating polyacids. *Prog. Polym. Sci.* **112**, 101322 (2021).
94. S. Adhikari, M. A. Leaf, M. Muthukumar, Polyelectrolyte complex coacervation by electrostatic dipolar interactions. *J. Chem. Phys.* **149**, 163308 (2018).
95. A. Salehi, R. G. Larson, A molecular thermodynamic model of complexation in mixtures of oppositely charged polyelectrolytes with explicit account of charge association/dissociation. *Macromolecules* **49**, 9706–9719 (2016).
96. T. K. Lytle, C. E. Sing, Transfer matrix theory of polymer complex coacervation. *Soft Matter* **13**, 7001–7012 (2017).
97. E. W. Martin *et al.*, A multi-step nucleation process determines the kinetics of prion-like domain phase separation. *Nat. Commun.* **12**, 4513 (2021).
98. M. Kar *et al.*, Phase-separating RNA-binding proteins form heterogeneous distributions of clusters in subsaturated solutions. *Proc. Natl. Acad. Sci. U.S.A.* **119**, e2202222119 (2022).
99. A. N. Milin, A. A. Deniz, Reentrant phase transitions and non-equilibrium dynamics in membraneless organelles. *Biochemistry* **57**, 2470–2477 (2018).
100. A. Plumridge, S. P. Meisburger, L. Pollack, Visualizing single-stranded nucleic acids in solution. *Nucleic Acids Res.* **45**, e66 (2017).
101. K. D. Kumble, A. Kornberg, Inorganic polyphosphate in mammalian cells and tissues. *J. Biol. Chem.* **270**, 5818–5822 (1995).
102. A. H. Phillips, R. W. Kriwacki, Intrinsic protein disorder and protein modifications in the processing of biological signals. *Curr. Opin. Struct. Biol.* **60**, 1–6 (2020).
103. C. W. Pak *et al.*, Sequence determinants of intracellular phase separation by complex coacervation of a disordered protein. *Mol. Cell* **63**, 72–85 (2016).
104. H. J. Dyson, Roles of intrinsic disorder in protein–nucleic acid interactions. *Mol. Biosyst.* **8**, 97–104 (2012).
105. N. Korolev, A. Allahverdi, A. P. Lyubartsev, L. Nordenskiold, The polyelectrolyte properties of chromatin. *Soft Matter* **8**, 9322–9333 (2012).
106. D. Nettels *et al.*, Single molecule spectroscopy of the temperature-induced collapse of unfolded proteins. *Proc. Natl. Acad. Sci. U.S.A.* **106**, 20740–20745 (2009).
107. D. Nettels, B. Schuler, Fretica. GitHub. https://github.com/SchulerLab/Fretica.git. Accessed 17 September 2023.
108. K.-I. Tainaka, Effect of counterions on complex coacervation. *Biopolymers* **19**, 1289–1298 (1980).
109. D. Priftis, M. Tirrell, Phase behaviour and complex coacervation of aqueous polypeptide solutions. *Soft Matter* **8**, 9396–9405 (2012).
110. R. Chollakup, W. Smitthipong, C. D. Eisenbach, M. Tirrell, Phase behavior and coacervation of aqueous poly(acrylic acid)—poly(allylamine) solutions. *Macromolecules* **43**, 2518–2528 (2010).
111. A. Salehi, P. S. Desai, J. Li, C. A. Steele, R. G. Larson, Relationship between polyelectrolyte bulk complexation and kinetics of their layer-by-layer assembly. *Macromolecules* **48**, 400–409 (2015).
112. T. Farhat, G. Yassin, S. T. Dubas, J. B. Schlenoff, Water and ion pairing in polyelectrolyte multilayers. *Langmuir* **15**, 6621–6623 (1999).
113. J. R. Vieregg *et al.*, Oligonucleotide-peptide complexes: Phase control by hybridization. *J. Am. Chem. Soc.* **140**, 1632–1638 (2018).
114. P. Schaaf, J. B. Schlenoff, Saloplastics: Processing compact polyelectrolyte complexes. *Adv. Mater.* **27**, 2420–2432 (2015).
115. Q. Wang, J. B. Schlenoff, The polyelectrolyte complex/coacervate continuum. *Macromolecules* **47**, 3108–3116 (2014).
116. S. Meng, J. M. Ting, H. Wu, M. V. Tirrell, Solid-to-liquid phase transition in polyelectrolyte complexes. *Macromolecules* **53**, 7944–7953 (2020).
117. S. L. Perry *et al.*, Chirality-selected phase behaviour in ionic polypeptide complexes. *Nat. Commun.* **6**, 6052 (2015).
118. A. Vidyasagar, C. Sung, R. Gamble, J. L. Lutkenhaus, Thermal transitions in dry and hydrated layer-by-layer assemblies exhibiting linear and exponential growth. *ACS Nano* **6**, 6174–6184 (2012).
119. Y. Chen, M. Yang, J. B. Schlenoff, Glass transitions in hydrated polyelectrolyte complexes. *Macromolecules* **54**, 3822–3831 (2021).